Electronic Supplementary Material (ESI) for Nanoscale.

Supplementary materials

Modulated Interlayer Charge transfer dynamics in monolayer TMD/metal junction

Linglong Zhang,[*] [*][a, b] Han Yan,[*b] Xueqian Sun,[*b] Miheng Dong,[b] Tanjun Yildirim,[b] Bowen Wang,[b] Bo Wen,[b] Guru Prakash Neupane,[b] Ankur Sharma,[b] Yi Zhu, [b] Jian Zhang,[b] Kun Liang, [b] Boqing Liu, [b] Hieu T. Nguyen,[b] Daniel Macdonald,[b] Yuerui Lu[*] [b]

[a.] *National Laboratory of Solid State Microstructures, Collaborative Innovation Center of Advanced Microstructures, School of Electronic Science and Engineering, Nanjing University, Nanjing 210093, People's Republic of China.*

[*.] *E-mail：linglong.zhang@yahoo.com*

[b.] *Research School of Engineering, College of Engineering and Computer Science, the Australian National University, Canberra, ACT 2601, Australia.*

[*.] *E-mail：yuerui.lu@anu.edu.au*

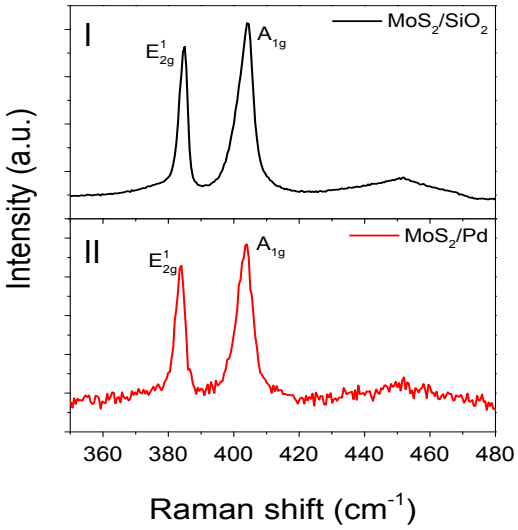

Fig. S1 Confirmation of the structure of 1L MoS_2/Pd. Raman spectra of 1L MoS_2/SiO_2 (I) and 1L MoS_2/Pd junction (II) at room temperature confirming monolayer MoS_2.

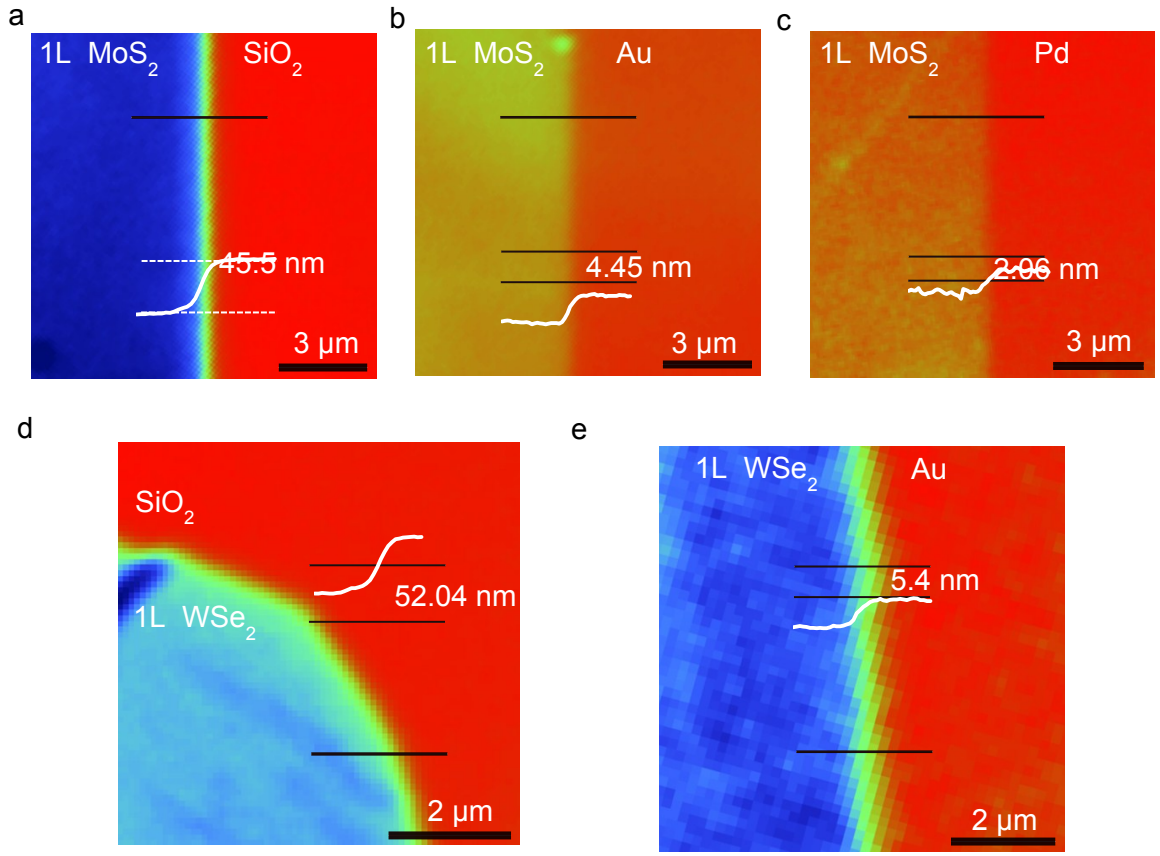

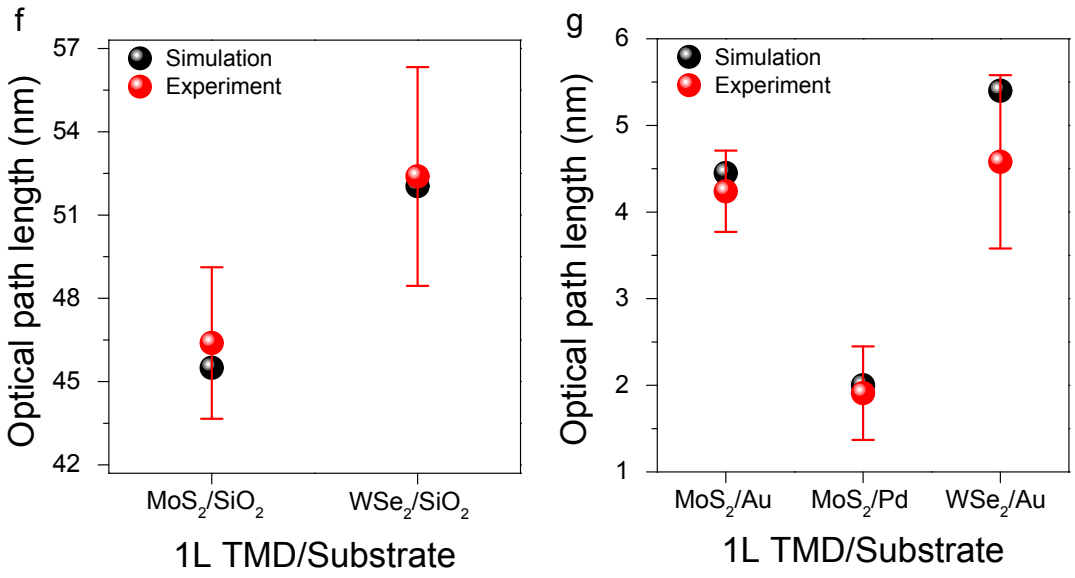

Fig. S2 a, PSI Characterizations of 1L TMD on the different substrates. a, PSI image of 1L MoS_2 on SiO_2. **b,** PSI image of 1L MoS_2 on Au**. c,** PSI image of 1L MoS_2 on Pd. Scale bar is 3 μm. **d,** PSI image of 1L WSe_2 on SiO_2. Scale bar is 2 μm. Here, we presented the data of WSe_2 on different substrates for comparison. **e,** PSI image of 1L WSe_2 on Au. Scale bar is 2 μm. **f,** Experimental statistics and simulation data representations of the optical path lengths (OPL) from monolayer TMD on the SiO_2/Si substrates. **g,** Experimental statistics and simulation data representations of the optical path lengths (OPL) from monolayer TMD on the various metal substrates. The values were then used to calibrate the thickness of monolayer TMD using at least two sets of measurements on each sample. The actual thickness of monolayer TMD was confirmed using AFM[1,2]. Red ball shows the experimental data and black balls show the simulated value.

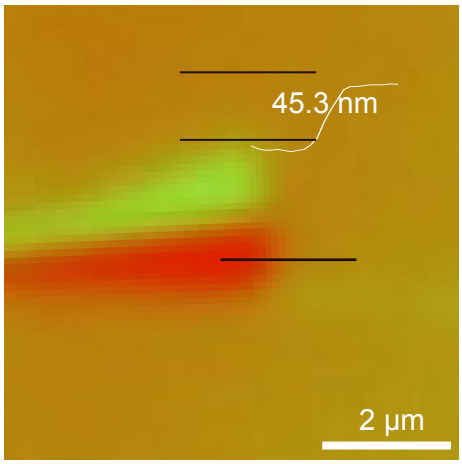

Fig. S3 Confirmation of 1L MoS_2/Pd junction. PSI image of the dash lined region in Figure 1c (II) showing the optical length of monolayer MoS_2. Scal e bar is 2 µm.

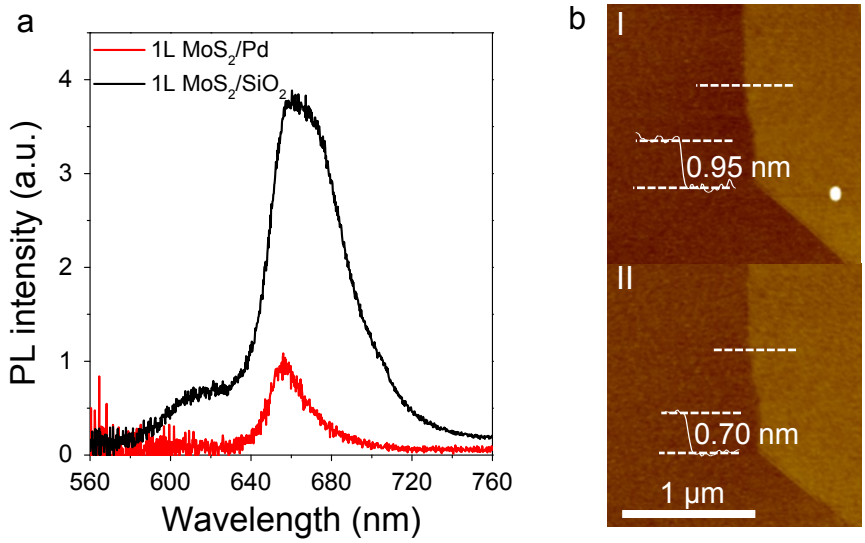

Fig. S4 Annealing effects a, Room-temperature PL spectra of 1L MoS_2/SiO_2 and 1L MoS_2/Pd junction after annealing showing a quenching factor η of 10.3. ***b, (I), (II),*** *AFM characterizations before annealing (I) and after annealing (II) of monolayer MoS_2 onto Pd substrate. It shows a thickness change of around 0.25 nm.*

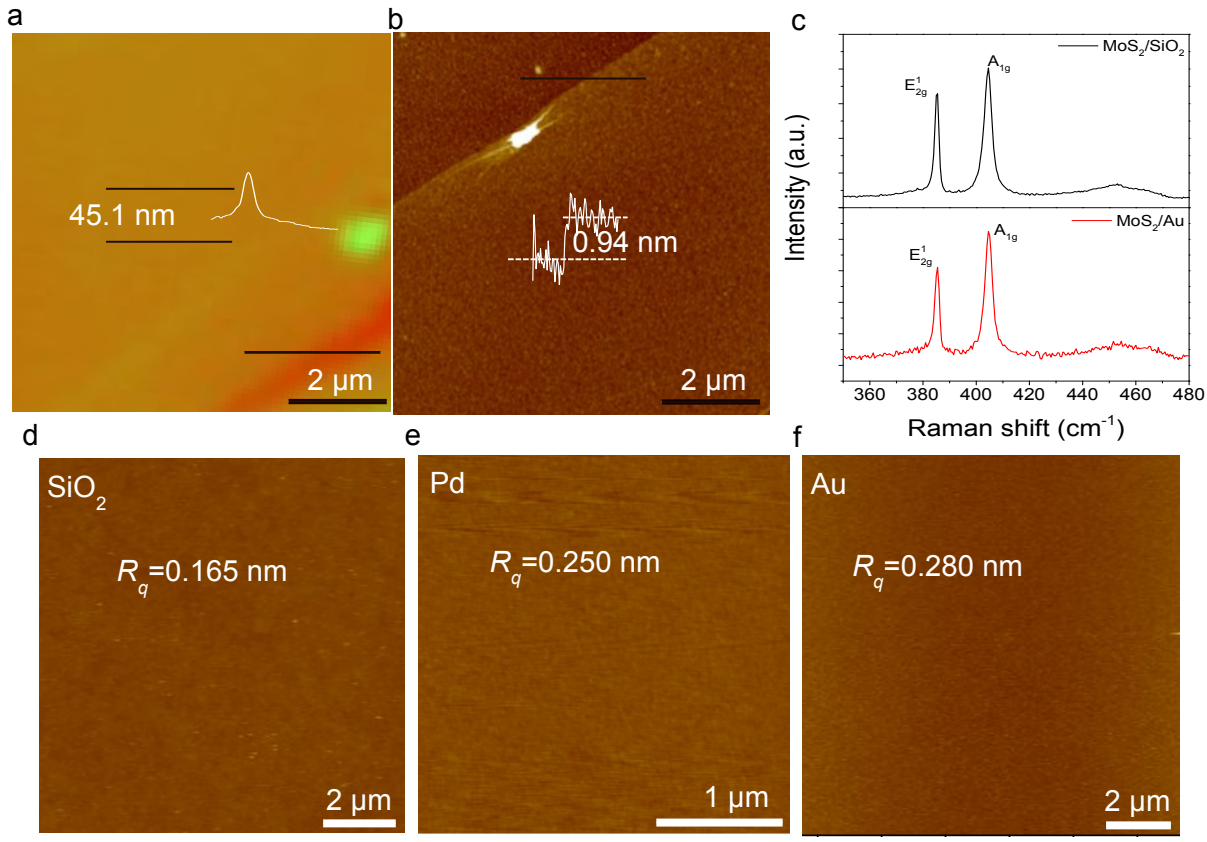

Fig. S5 Confirmation of 1L MoS_2/Au junction. **a**, PSI image of the dotted rectangular area (I) shown in **Figure 3a**. Inset: Height measurements along the dashed line showing atomic layer thickness. Scale bar, 2 μm. **b**, AFM image of the dotted rectangular area (II) shown in **Figure 3a**. Inset: Height measurements along the dashed line showing atomic layer thickness. Scale bar 2 μm. **c,** Raman spectra of 1L MoS_2/SiO_2 (top panel) and 1L MoS_2/Au (bottom panel) hybrid system at room temperature. ***d****, AFM scan of SiO_2 substrate showing Root mean square roughness (R_q) of ~0.165 nm.* ***b****. AFM scan of Pd substrate showing R_q of ~ 0.250 nm.* ***c****. AFM scan of Au substrate showing R_q of ~ 0.280 nm. Metal substrates show small R_q, which is comparable to SiO_2 Substrate, critical for the stability and repeatability of measurements.*

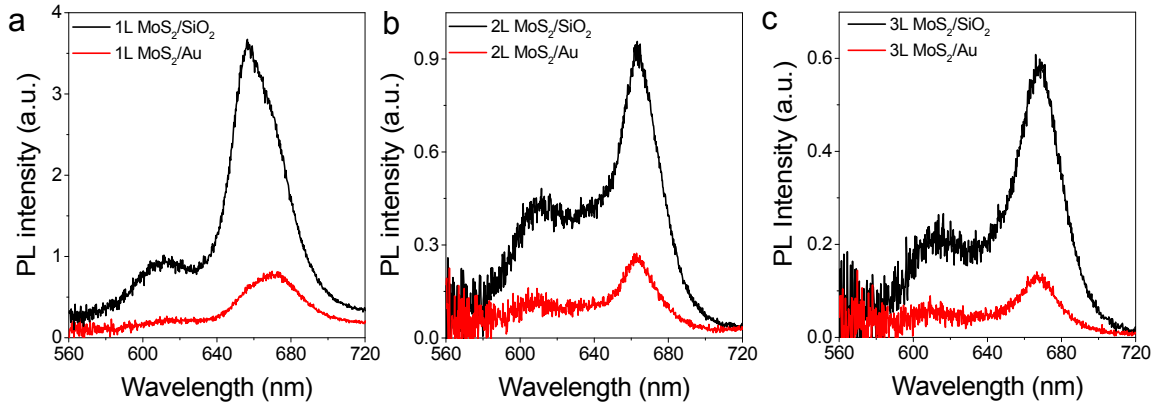

Fig. S6 Thickness modulation ***a****, PL spectra from 1L MoS_2/SiO_2 and 1L MoS_2/Au junctions at room temperature showing PL quenching factor of ~3.94.* ***b****, PL spectra from 2L MoS_2/SiO_2 and 2L MoS_2/Au junctions at room temperature showing PL quenching factor of ~3.23.* ***c****, PL spectra from 3L MoS_2/SiO_2 and 3L MoS_2/Au junctions at room temperature showing PL quenching factor of ~2.58.* Intriguingly, *among them, we observed that the quenching factor η decreases with the increase of MoS_2 thickness. We ascribed it to the deccrease of the tunneling efficiency with increasing thickness of MoS_2.[3] On the other hand, the increased mobility in MoS_2 with thickness may contribute as well.[3-5]*

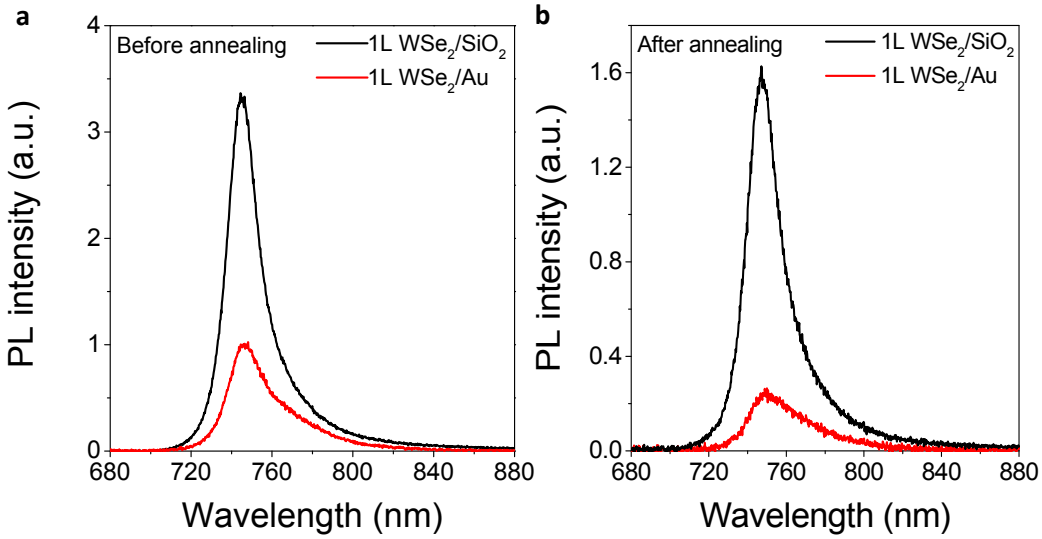

Fig. S7 Other TMD/metal junctions ***a****, Room-temperature PL spectra of 1L WSe_2/SiO_2 and 1L WSe_2/Au junction before annealing showing a quenching factor η of 2.43.* ***b****, Room-*

temperature PL spectra of 1L WSe_2/SiO_2 and 1L WSe_2/Au junction after annealing showing a quenching factor η of 4.57. This demonstrates similar observations with monolayer WSe_2 compared to MoS_2 based junctions.

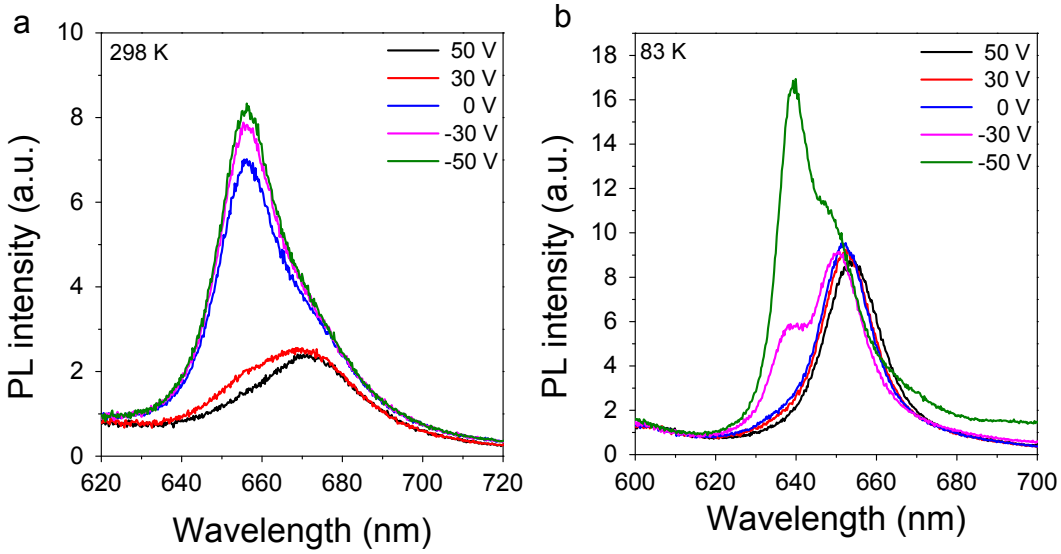

Fig. S8 Exciton and trion of monolayer MoS_2. a, PL intensity as a function of back gate voltage from 1L MoS_2 at room temperature. **b**, PL intensity as a function of back gate voltage from 1L MoS_2 at 83 K.

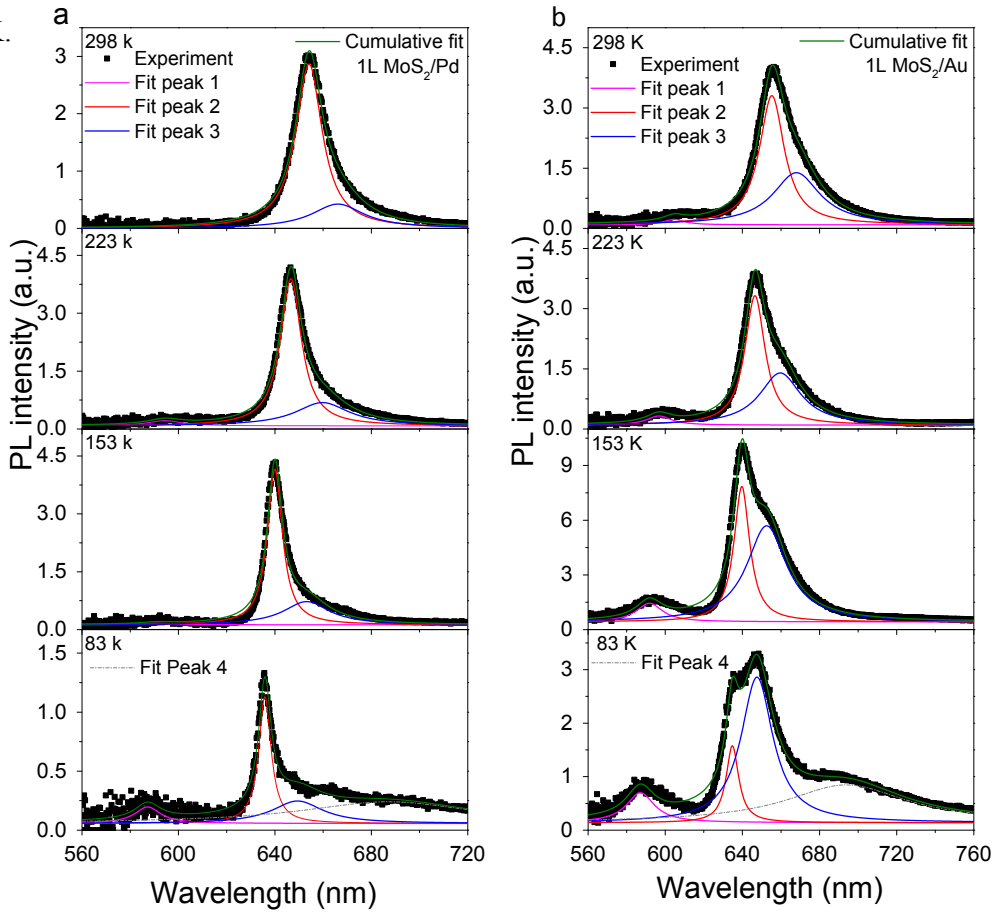

Fig. S9 PL spectra fitting. a, Fitting of PL spectra from 1L MoS_2/Pd as a function of temperature. The PL spectra were fitted by a Lorenz function (Black scatter lines are the experimental data, magenta lines are labelled as Fit Peak 1 representing *B* exciton peak, red lines are labelled as Fit Peak 2 representing *A* exciton peak, blue lines are labelled as Fit Peak 3 representing A^- trion peak, grey dashed lines are labelled as Fit Peak 4 representing defect peak, and olive line is labelled as Cumulative Fit.) **b**, Fitting of PL spectra from 1L MoS_2/Au as a function of temperature. The PL spectra were fitted by Lorenz function (Black scatter lines are the experimental data, magenta lines are labelled as Fit Peak 1 representing *B* exciton peak, red lines are labelled as Fit Peak 2 representing *A* exciton peak, blue lines are labelled as Fit Peak 3 representing *A* trion peak, grey dashed lines are labelled as Fit Peak 4 representing defect peaks, and olive line is labelled as Cumulative Fit.)

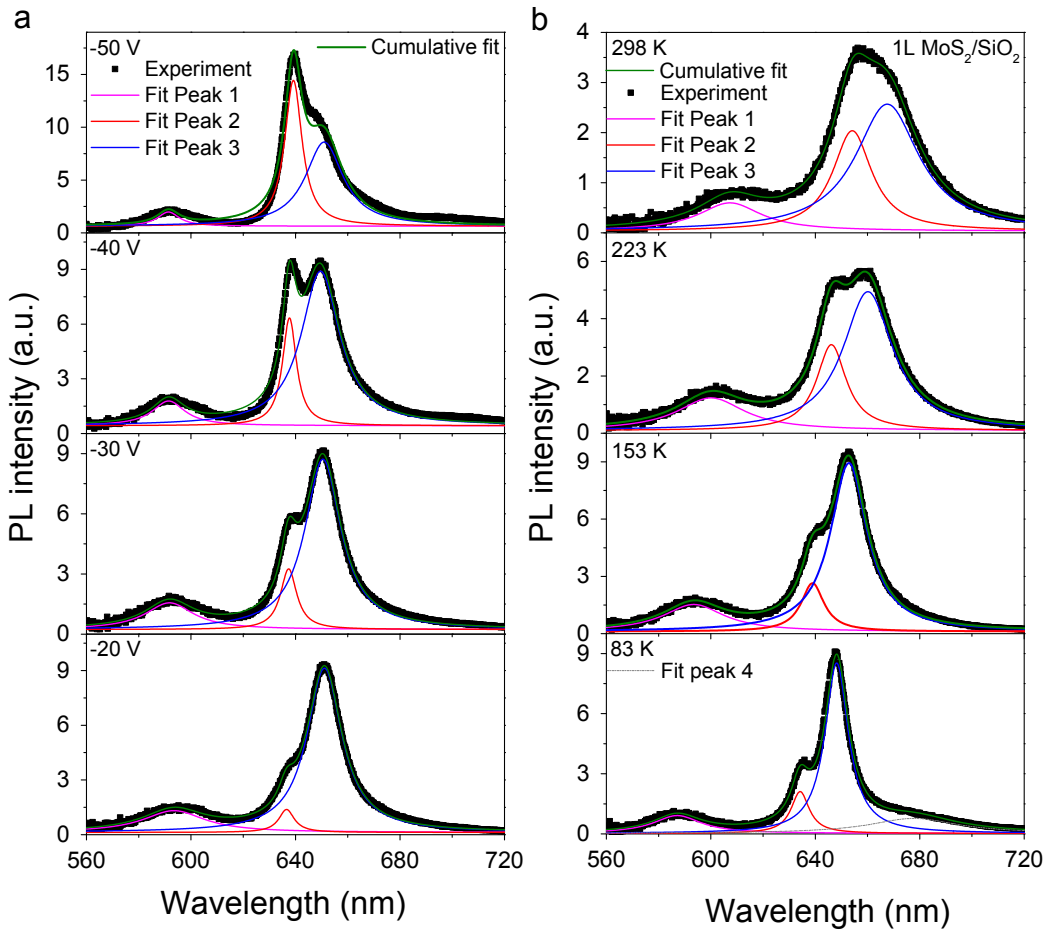

Fig. S10 PL spectra fitting. a, Fitting of the PL spectra at the gate voltage of ranging from -50 V to -20 V at 83 K. This shows the neutral excitons could be observed with the large hole (negative voltage) doping. **b**, Fitting of PL spectra from 1L MoS_2/SiO_2 as a function of temperature. The PL spectra were fitted by Lorenz function (Black scatter lines are the experimental data, magenta lines are labelled as Fit Peak 1 representing *B* exciton peak, red lines are labelled as Fit Peak 2 representing *A* exciton peak, blue lines are labelled as Fit Peak 3 representing *A* trion peak, grey dashed lines are labelled as Fit Peak 4 representing defect peak, and olive line is labelled as Cumulative Fit.)

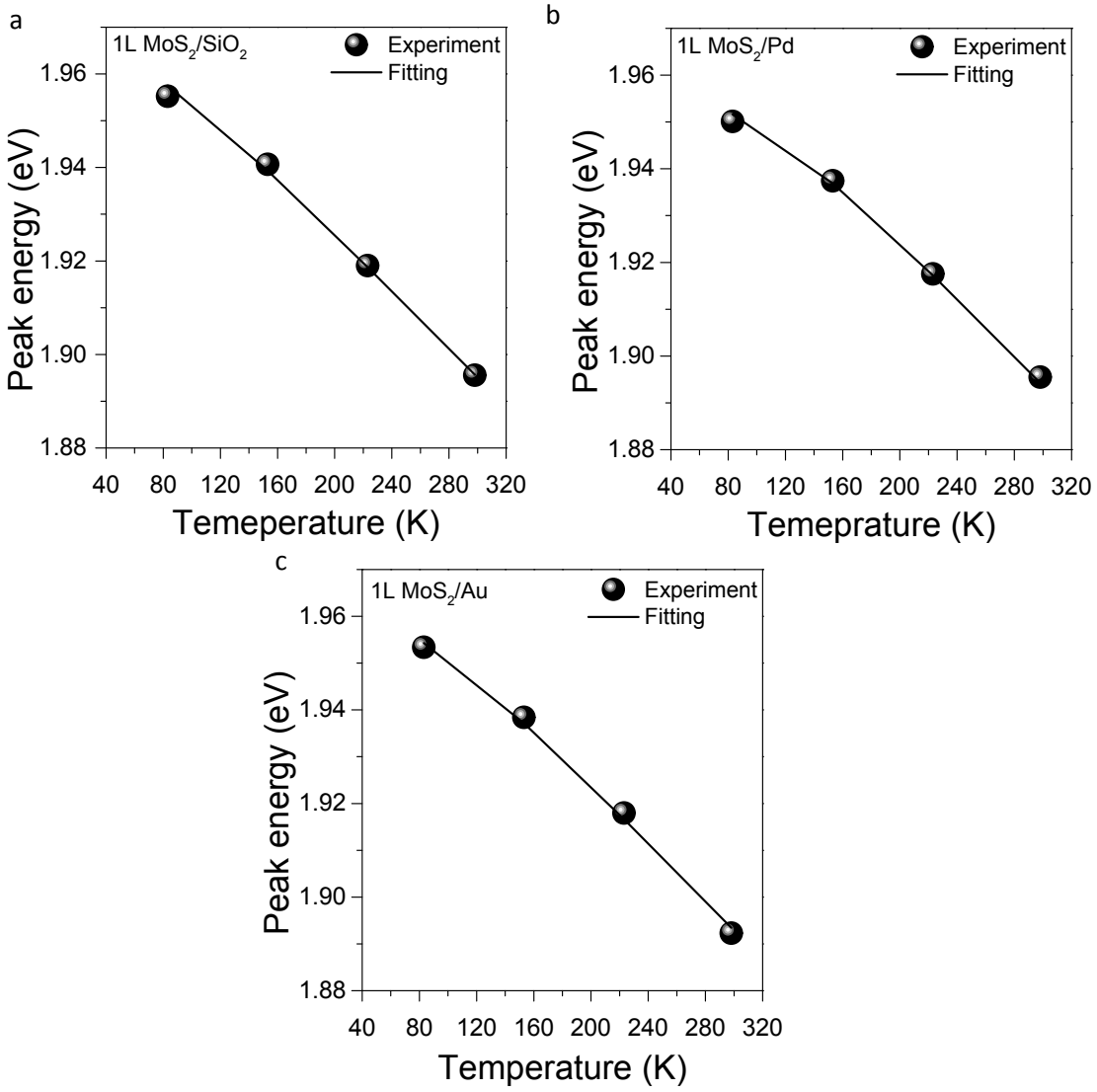

Fig. S11 Temperature-dependent A peak energy. a, Peak energy of *A* exciton as a function of temperature in 1L MoS_2/SiO_2 structure. The solid line is the fitting curves. Here, *A* peak energy was

extracted from Figure S10b. **b**, Peak energy of *A* exciton as a function of temperature in 1L MoS_2/Pd structure which was extracted from Figure S9a. The solid line is the fitting curves. **c**, Peak energy of *A* exciton as a function of temperature in 1L MoS_2/Au junction which was extracted from Figure S9b. The solid line is the fitting curves.

Supplementary note S1: PSI calibration

We employed the phase-shift interferometry (PSI) system to measure the optical path length (OPL) of the 2D layers.[6] The OPL is determined through the relation: $OPL_i = -\frac{\lambda}{2\pi}(\emptyset_i - \emptyset_{sub})$, where λ is the wavelength of the light source (i.e., 535 nm), $\emptyset_i$ and $\emptyset_{sub}$ represent the measured phase-shifts of the reflected light signal from the monolayer TMD and the substrate, respectively.[7] It has been demonstrated that the PSI system with a high resolution of ~0.1 nm in the detection of surface profile, is a sensitive and powerful tool to characterise atomically thin materials.[7] The corresponding measured OPL values of 1L MoS_2 on SiO_2, 1L WSe_2 on SiO_2 are ~46.3 and 52.4 nm (Figure S2). Furthermore, the OPL values of 1L MoS_2 on Pd, 1L MoS_2 on Au and 1L WSe_2 on Au were also measured to be ~1.9, 4.2 and 4.6 nm, respectively. In addition, the numerical simulation based on the Standford stratified Structure Solver (S4)[8] was performed to calculate the OPL values for mTMD on three different substrates, including SiO_2/Si, Gold and Palladium (Figure S2f and S2g). The simulation process numerically solves the Maxwell's equation of the multiple layer structure by expanding the field in Fourier-space. In the calculation, the refractive index values of SiO_2, Si, 1L MoS_2, 1LWSe_2, Pd and Au is set to 1.46,[9] 4.15+0.05i,[10,11] 5.3+1.3i,[7] 5.64+1.29i,[12] 0.48+4.14i,[13] 0.54+2.21i,[14] respectively. The measured and simulated OPL value consists well with each other (Figure S2f and S2g).

Supplementary note S2: Quenching factor fitting

The interlayer interaction is exponentially on the interlayer spacing while the variation of the interlayer spacing (i.e., tunnel barrier width *d*) with temperature is virtually non-linear.[15,16] Therefore, tunnel barrier width *d* could be defined as: $d=at^2+bt+c$, in unit of Å, where *a, b* and *c* are fitting parameters. Therefore the quenching factor (η), reflecting the coupling strength, could be described as:

$$\eta \propto exp(-(at^2 + bt + c)) \quad \text{(S1)}$$

In Figure 2b and 3b, the fitting and experiment data of η from 1L MoS_2 on metal (e.g., Pd and Au) junction have been plotted and match very well.

Supplementary note S3: FWHM analysis

As shown in Figure 3c, the FWHM of the three structures shows a similar increasing trend as the temperature increases. In contrast, the 1L MoS_2/Pd junction always keeps the smallest FWHM than the other two structures. It is accepted that the total linewidth obtained could be explained in the following equation:[1,17]

$$\acute{\Gamma}(T) = \acute{\Gamma}_{0+} + \sigma T + \acute{\Gamma}_{LO}\left(exp\left(\frac{E_{LO}}{K_B T}\right) - 1\right)^{-1} \quad \text{(S2)}$$

Here, $\acute{\Gamma}_{0+}$ is the dominantly electron-electron scattering representing term, which is independent on the temperature. σ is the electron-acoustic/thermal phonon coupling coefficient. $\acute{\Gamma}_{LO}$ represents the exciton-*LO* phonon coupling strength. E_{LO} is the *LO* phonon energy. Given the second and third term of the expression S2, we could explain that FWHM would increases with the increasing temperature. This could be qualitatively explained that exciton scattering by acoustic and optical phonons enhanced when the temperature increased.[1,17,18]

Supplementary note S4: Doping level estimation

Firstly, we employed the three-level model to analyze the PL intensity of excitons (*A*) and trions (A^-) among the three junctions. The rate equations for the population of exciton N_A and N_{A^-} could be expressed as

$$\frac{dN_A}{dt} = G - \left\{\Gamma_A^{'} + k_{A^-}\right\}N_A \quad \text{(S3)}$$

$$\frac{dN_{A^-}}{dt} = k_{A^-} N_A - \Gamma_{A^-} N_{A^-} \quad \text{(S4)}$$

where k_{A^-} denotes the formation rate of the trion from the exciton, and *G* represents the optical generation rate of excitons. The population of excitons and trions in the steady-state solutions of the Eqs. (S3) and (S4) could be expressed as

$$N_A = \frac{G}{\Gamma_A^{'} + k_{A^-}} \quad \text{(S5)}$$

$$N_{A^-} = \frac{k_{A^-} \quad G}{\Gamma_{A^-} \Gamma_A^{'} + k_{A^-}} \quad \text{(S6)}$$

where $\Gamma_A^{'}$ and Γ_{A^-} represents the decay rates of the exciton and trion, respectively. The PL intensity of the exciton (I_A) and trion (I_A^-) could be expressed according to the relationship where PL intensity is proportional to the exciton (trion) populations as follows:

$$I_A = \frac{\alpha G \gamma_A}{\Gamma_A^{'} + k_{A^-}} \quad \text{(S7)}$$

$$I_{A^-} = \frac{k_{A^-} \quad \alpha G \gamma_{A^-}}{\Gamma_{A^-} \Gamma_A^{'} + k_{A^-}} \quad \text{(S8)}$$

where γ_A and γ_{A^-} is the radiative decay rate of the exciton and trion, respectively. For simplicity, the change of these values with the metal contact doping is assumed to be small and negligible in the analysis.[18,19] Hence, we assume that the radiative decay rate of the exciton is independent on the carrier density. The coefficient α expresses the collection efficiency of the luminescence. The parameters $\Gamma_A^{'} = 0.002$ ps^{-1}, $\Gamma_{A^-} = 0.002$ ps^{-1}, and k_{A^-}=0.5 ps^{-1} values were extracted from transient absorption measurements in previous studies.[19,20] Moreover, $\alpha G \gamma_A e$and $\alpha G \gamma_{A^-}$ was extracted to be 10 and 1.5, respectively, which

is consistent with earlier reports for monolayer MoS_2.[19] Herein, $k_{A^-}\Gamma_A^{'}$, the PL intensity of the exciton (I_A) and trion (I_A-) could be approximately described as

$$I_A = \frac{\alpha G \gamma_A}{k_{A^-}} \tag{S9}$$

$$I_{A^-} = \frac{\alpha G \gamma_{A^-}}{\Gamma_{A^-}} \tag{S10}$$

In addition, the mass action model correlated to the trions, was applied to evaluate the doped density in monolayer MoS_2 from the three junctions. According to the above scheme, the relationship between the density and trion binding energy E_b was obtained:[19]

$$\frac{N_A n_{el}}{N_{A^-}} = (\frac{4 m_A m_e}{\pi \hbar^2 m_{A^-}}) K_B T exp(-\frac{E_b}{K_B T}) \tag{S11}$$

where T is temperature, K_B denotes Boltzmann constant, E_b is the trion binding energy (~20 meV), which was measured in our experiments, consisting well with the earlier studies.[18,19] m_e ($0.35m_0$) and m_h ($0.45m_0$) represents the effective mass of electrons and holes, respectively, in which m_o denotes the free electron mass. The effective masses of an exciton m_A and the trion m_{A^-} coud be calculated as $0.8m_0$ and $1.15m_0$, respectively. Using these parameters and combining Eqs. (S5)–(S7) with Eq. (S8), the trion PL intensity weight is described as:

$$\frac{I_{A^-}}{I_{total}} = \frac{\frac{\gamma_{A^-} N_{A^-}}{\gamma_A \ N_A}}{1 + \frac{\gamma_{A^-} N_{A^-}}{\gamma_A \ N_A}} \approx \frac{4 \times 10^{-14} n_{el}}{1 + 4 \times 10^{-14} n_{el}} \tag{S12}$$

The correlated doping level from various heterojunctions was presented in Figure 3f *via* Rq. (S4).

Supplementary note S5: Estimation of exciton-phonon coupling

The peak energy of an *A* exciton would experience a blueshift with a decrease of the temperature (Figure S9 and S10b).[21] This is due to the renormalization of band energy by electron-phonon interaction induced by the change of the temperature, while thermal expansion could be negligible.[21] By employing the modified Varshi relation, the temperature dependence of the *A* exciton peak energy is fitted using[1,17,21]:

$$E(T) = E_0 - S < \hbar\omega > \left[coth\frac{< \hbar\omega >}{2K_B T} - 1 \right] \quad \text{(S13)}$$

where all used parameters are consistent with the main text. Table S1 lists the used parameters in the fitting of the three structures. Here, the 1L MoS_2/Pd has the largest *S* value of 1.96 which is larger than that of 1L MoS_2/Au (1.90) and 1L MoS_2/SiO_2 (1.85) and this implies the strongest coupling of 1L MoS_2/Pd.[21]

Table S1 Used parameters of exciton-phonon coupling

Name	$E_g(0)$ (eV)	$<\hbar\omega>$ (meV)	*S*
1L MoS_2/SiO_2	1.96	15.50	1.85
1L MoS_2/Pd	1.96	24.10	1.96
1L MoS_2/Au	1.96	18.60	1.90

Reference

1. A. Sharma, B. Wen, B. Liu, Y. W. Myint, H. Zhang and Y. Lu, *Small*, 2018, 8.
2. S. Tongay, J. Suh, C. Ataca, W. Fan, A. Luce, J. S. Kang, J. Liu, C. Ko, R. Raghunathanan, J. Zhou, F. Ogletree, J. Li, J. C. Grossman and J. Wu, *Scientific reports*, 2013, **3**, 2657.
3. J. Kang, W. Liu, D. Sarkar, D. Jena and K. Banerjee, *Physical Review X*, 2014, **4**.
4. L. Zhang, A. Sharma, Y. Zhu, Y. Zhang, B. Wang, M. Dong, H. T. Nguyen, Z. Wang, B. Wen, Y. Cao, B. Liu, X. Sun, J. Yang, Z. Li, A. Kar, Y. Shi, D. Macdonald, Z. Yu, X. Wang and Y. Lu, *Advanced materials*, 2018, e1803986.
5. S. Ghatak, A. N. Pal and A. Ghosh, *Acs Nano*, 2011, **5**, 7707-7712.
6. R. Xu, J. Yang, Y. Zhu, H. Yan, J. Pei, Y. W. Myint, S. Zhang and Y. Lu, *Nanoscale*, 2016, **8**, 129-135.
7. J. Yang, R. Xu, J. Pei, Y. W. Myint, F. Wang, Z. Wang, S. Zhang, Z. Yu and Y. Lu, *Light: Science & Applications*, 2015, **4**, e312.
8. V. Liu and S. Fan, *Computer Physics Communications*, 2012, **183**, 2233-2244.
9. I. H. Malitson, *Journal of the Optical Society of America*, 1965, **55**, 5.
10. D. E. Aspnes and A. A. Studna, *Physical Review B*, 1983, **27**, 985-1009.
11. J. H. Kim, S. H. Ehrman, G. W. Mulholland and T. A. Germer, *Applied optics*, 2002, **41**, 8.
12. H. Liu, C. Shen, S. Su, C. Hsu, M. Li and L. Li, *Applied Physics Letters*, 2014, **105**, 201905.
13. W. S. M. Werner, K. Glantschnig and C. Ambrosch-Draxl, *Journal of Physical and Chemical Reference Data*, 2009, **38**, 1013-1092.
14. P. B. Johnson and R. W. Christy, *Physical Review B*, 1972, **6**, 4370-4379.
15. P. L. Walker, H. A. M. Jr. and C. C. Wright, *Industrial and Engineering Chemistry* 1953, **45**, 5.

16. E. G. Steward, B. P. Cook and E. A. Kellett, *Nature*, 1960, **187**, 2.
17. X. Wen, A. Sitt, P. Yu, Y. R. Toh and J. Tang, *Physical chemistry chemical physics : PCCP*, 2012, **14**, 3505-3512.
18. Y. Li, Z. Qi, M. Liu, Y. Wang, X. Cheng, G. Zhang and L. Sheng, *Nanoscale*, 2014, **6**, 15248-15254.
19. S. Mouri, Y. Miyauchi and K. Matsuda, *Nano letters*, 2013, **13**, 5.
20. H. Shi, R. Yan, S. Bertolazzi, J. Brivio, B. Gao, A. Kis, D. Jena, H. G. Xing and L. Huang, *Acs Nano*, 2013, **7**, 9.
21. F. Wang, J. Wang, S. Guo, J. Zhang, Z. Hu and J. Chu, *Scientific reports*, 2017, **7**, 44712.